

Article

Theoretical Studies on Hydrogen Bonds in Anions Encapsulated by an Azamacrocyclic Receptor

Jing Wang ¹, Jiande Gu ², Md. Alamgir Hossain ³ and Jerzy Leszczynski ^{1,*}

¹ Interdisciplinary Nanotoxicity Center, Department of Chemistry, Jackson State University, Jackson, MS 39217, USA; jingw@icnanotox.org

² Drug Design & Discovery Center, State Key Laboratory of Drug Research, Shanghai Institute of Materia Medica, Chinese Academy of Sciences, Shanghai 201203, China; jiande@icnanotox.org

³ Department of Chemistry and Biochemistry, Jackson State University, Jackson, MS 39217, USA; md.a.hossain@gmail.com

* Correspondence: jerzy@icnanotox.org; Tel.: +1-601-979-3482

Academic Editor: Sławomir J. Grabowski

Received: 31 January 2016; Accepted: 16 March 2016; Published: 22 March 2016

Abstract: Hydrogen bonds in two halides encapsulated by an azamacrocyclic receptor were studied in detail by the density functional theory (DFT) approaches at B3LYP/6-311++G(d,p) and M06-2X/6-311++G(d,p) levels. The atoms in molecules (AIM) theory and the electron density difference maps were applied for characterizing the hydrogen bond patterns. The results suggest that the fluoride complex has a unique binding pattern which shows a hydrogen bond augmented with ionic bond characteristics.

Keywords: hydrogen bonds; halides; azamacrocyclic receptor; DFT

1. Introduction

The specific interactions between anions and their supramolecular receptors have been widely studied [1–4]. Among the various anions, halides play an important role in environments and life [5]. Interactions between halides and synthetic receptors have been broadly investigated both experimentally and theoretically [2,6–12]. Studies indicate that these interactions are mainly attributed to hydrogen bonding and electrostatic attractions. The binding patterns and selectivity vary with different spacers and the linking amine groups [13–16].

A simple monocyclic polyamine incorporated with *N*-methyl-2,2'-diaminodiethylamine may selectively encapsulate a sulfate anion through multiple hydrogen bonds [17]. Studies reported that this receptor was able to encapsulate two chlorides in its macrocyclic cavity as well [18]. The X-ray crystallography structure of the charge-assisted two chlorides encapsulated by a hexaprotonated azamacrocycle ($[H_6L]^{6+}$) demonstrates that two chlorides are located on the opposite side of the macrocycle through trigonal recognition by hydrogen-bonding interactions [19]. Hence, the interactions for this receptor and halides were further investigated by experiments and theoretical methods [20]. The binding between halide and a *p*-xylyl-based azamacrocycle was studied experimentally by ¹H-NMR titrations and single crystal X-ray diffraction analysis. Meanwhile, the binding properties and the hydrogen bonds in the complexes were studied by density functional theory (DFT) at the M06-2X/6-311G(d,p) level. Both 1:1 and 1:2 complexes of $[H_6L(X)_2]^{4+}$ with halides were investigated. The 1:2 binding mode was found to be energetically favorable [19]. The structural analysis reveals that each halide forms three hydrogen bonds with the neighboring protonated amine nitrogen for each 1:2 halides binding complex. However, the predicted binding energies for complexes of $[H_6L(F)_2]^{4+}$ (−158.5 kcal/mol) are too strong for characterizing six hydrogen bonds. Considering that there are six H-F bonds in this complex and each H-F bonding energy amounts to 26.4 kcal/mol [19], it

is clear that these H-F bonds should not be classified as normal H bonds. To understand the selectivity of the azamacrocycle it is necessary to explore the nature of these halide-amine interactions.

To further understand and shed a light on such strong interactions between fluoride anions and the binding center (amine), their binding patterns have been analyzed based on the electron density formation approach. This approach is proved to be able to reveal the binding patterns at the very basic electron density level of theory. For comparison, the atom in molecule (AIM) approach has also been applied to compensate the quantitating the binding patterns [21,22]. To avoid the bias of the specific DFT functional, both B3LYP/6-311++G(d,p) and M06-2X/6-311++G(d,p) methods were applied for all the structure optimizations and the electron density calculations and analysis.

2. Computational Methods

The density functional theory (DFT)-based calculations were carried out for the anion-bound azamacrocycle compounds. The DFT approach through Becke's three parameter (B3) exchange functional along with the Lee-Yang-Parr (LYP) nonlocal correlation functional B3LYP [20,23–25] with an optimized weight of the exact HF exchange was applied in the present study. The Minnesota density functional M06-2X [26–28] level calculations were also performed. The pseudopotential basis set LanL2DZ was applied for iodine. The standard valence triple zeta basis set, augmented with d-type polarization and diffuse functions for heavy elements, and p-type polarization and diffuse functions for H, 6-311++G(d,p) was used for all the other elements [29]. The Barone-Tomasi polarizable continuum model (PCM) [30] with the standard dielectric constant of water ($\epsilon = 78.39$) was applied to simulate the solvated environment of an aqueous solution. The force constants were determined analytically in the analysis of harmonic vibrational frequencies for all of the complexes. The GAUSSIAN 09 system of DFT programs [31] was used for all computations.

To analyze the H-bonding pattern in the anion-bonded azamacrocycle systems, the atoms-in-molecules (AIM) theory of Bader [21,22] was applied, and the analysis was performed by the AIM2000 program [32]. The AIM analysis is based upon the density obtained at the B3LYP/6-311++G(d,p) level. Hydrogen bonding can also be characterized by the change of the electron density for the bonded moiety. The electron density around the proton and the proton acceptor decreases, while the density between the proton and its acceptor increases as the results of the formation of a hydrogen bond [33].

3. Results and Discussions

The present studied models of $[\text{H}_6\text{L}(\text{X})_2]^{4+}$ have multiple charges. The interactions in the gas phase are mainly caused by the strong static electronic interactions between $[\text{H}_6\text{L}]^{6+}$ and the anions. In order to eliminate the influences of the static electronic interactions and reveal, more accurately, the hydrogen bonding, all the models were fully optimized including the solvent effects through the PCM model in which water is applied as the solvent. All the discussions will be focused on the results with solvent obtained using PCM models. The optimized structural parameters indicate that there is no significant difference between the structures predicted by the B3LYP method and those predicted by the M06-2X method (the largest deviations in the hydrogen bonding atomic distances are less than 0.02 Å, except for HB2 of $[\text{H}_6\text{L}(\text{F})_2]^{4+}$, which is 0.09 Å longer in the prediction with B3LYP than that with M06-2X). Therefore, the following discussion is mainly based on the results of the B3LYP/6-311++G(d,p) level of theory.

The azamacrocycle ring shows an ellipsoid structure, of which two methyl groups are trans-orientated. As shown in Figure 1, all six nitrogen atoms (from N1 to N6) are fully protonated. Studies show that two halide anions can be encapsulated in the azamacrocyclic cavity, forming stable 1:2 (ligand:anion) complexes [13]. Here we use the width and height values to describe the approximate size of the cavity. The atomic distance between N2 and N5 is used to represent the width of the azamacrocycle. The two aromatic benzene planes are parallel. The distance between the two parallel planes is used to describe the height of the cavity. The optimized cavity of the azamacrocycle has the

width of 9.966 Å and height of 6.838 Å. The fully-optimized structures of the halide-encapsulated azamacrocyclic complexes display symmetric geometry (C_{2h}). Six related hydrogen bonds are formed between the halides and the six neighboring protonated amine nitrogen for the complex, HB1, HB2, HB3, HB4, HB5, and HB6. Due to the structural symmetry, hydrogen bonds (HB4, HB5, HB6) have the same properties as hydrogen bonds of HB1, HB2, and HB3 (Figure 1). Therefore, in the following discussions, only HB1, HB2, and HB3 will be discussed in detail to avoid redundancy.

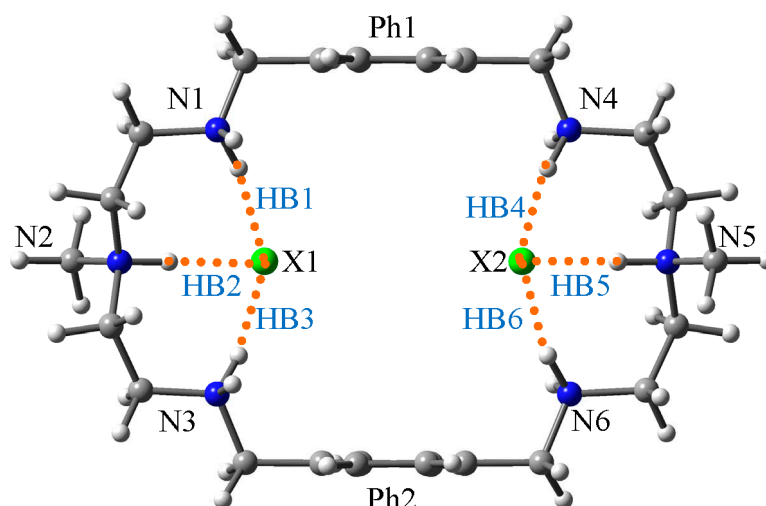


Figure 1. The scheme of the $[H_6L(X)_2]^{4+}$ structure. ($X = F^-$, Cl^- , Br^- , I^-).

3.1. Two Chlorides Encapsulated in $[H_6L]^{6+}$

The crystallography data of the chloride azamacrocyclic compound reveals that the host's cavity keeps the two chlorides inside with six hydrogen bonds [16]. Figure 2a shows the optimized structure resulted from the computations, which is highly consistent with that obtained from the X-ray data (see Supporting Information). In the theoretical structure, the width and the height of the cavity are calculated to be 10.768 Å and 7.927 Å, compared to the width and the height of 10.338 Å and 7.842 Å in the crystal structure (Table 1). The atomic distance of the chlorides is predicted to be around 5.628 Å, while in X-ray data the two chlorides are apart by about 4.433 Å. The atomic distance between N1 and Cl1 is predicted to be 3.172 Å (3.146 Å in crystal structure). In addition, the atomic distance between N2 and Cl1 is calculated to be 3.117 Å while the X-ray data reveals that the distance amounts to 3.067 Å. The binding energy for the chlorides with the azamacrocyclic cavity is predicted to be -52.2 kcal/mol.

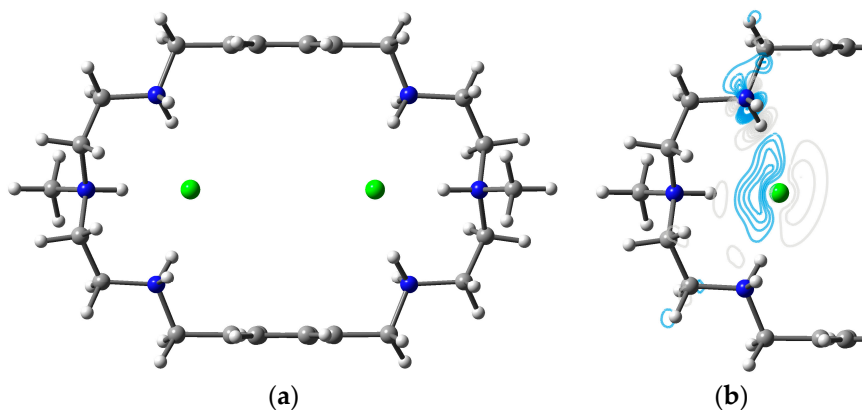


Figure 2. Cont.

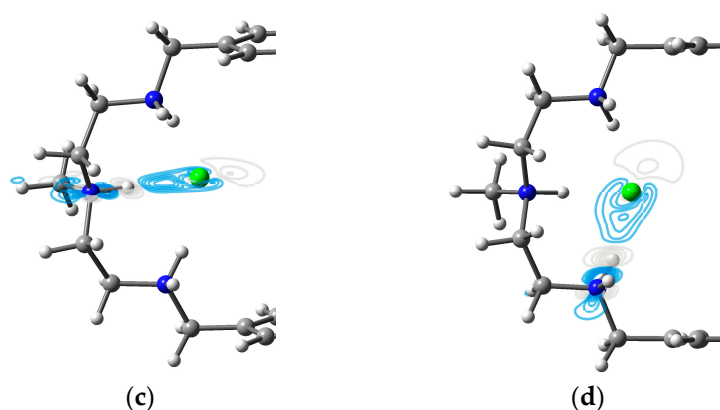


Figure 2. Two chlorides encapsulated by the azamacrocyclic compound (H_6L^{6+}). (a) Optimized $[\text{H}_6\text{LCl}_2]^{4+}$ structure; (b) electron density differences ($\Delta\rho$) maps of HB1 in the plane of N1-H-Cl1; (c) electron density differences ($\Delta\rho$) maps of HB2 in the plane of N2-H-Cl1; and (d) electron density differences ($\Delta\rho$) maps of HB3 in the plane of N3-H-Cl1. Contours in the deformation density map are shown at ± 0.001 au. Grey lines indicate deficiency of density, and blue lines indicate increasing density. $(\Delta\rho) = \rho[\text{H}_6\text{LCl}_2]^{4+} - \rho[\text{H}_6\text{L}]^{6+} - \rho(\text{Cl}_2)^{2-}$.

Table 1. Parameters for the hydrogen bonds at the B3LYP/6-311++G(d,p) level and AIM analysis (results at M06-2X/6-311++G(d,p) level are listed in parenthesis).

	Hydrogen Bonds	NH...X (Å)	$\rho(\text{BCPs})$ (au)	$\nabla^2\rho$ (au)	X...X (Å)	N2...N2' (Å)	H (Å)	ΔE (kcal/mol)	$\log K_2$ (Reference [19])
[H6L]F ₂	HB1	1.612 (1.627)	0.0514	0.0414					
	HB2	1.510 (1.413)	0.0691	0.0485	6.563 (6.502)	11.314 (11.106)	7.119 (7.172)	-95.9 (-108.9)	2.82
	HB3	1.612 (1.627)	0.0514	0.0414					
[H6L]Cl ₂	HB1	2.147 (2.130)	0.0296	0.0171					
	HB2	2.068 (2.049)	0.0368	0.0181	5.628 (5.628)	10.768 (10.678)	7.927 (7.736)	-52.2 (-66.5)	2.70
	HB3	2.147 (2.130)	0.0296	0.0171					
[H6L]Br ₂	HB1	2.311 (2.312)	0.0261	0.0135					
	HB2	2.233 (2.233)	0.0319	0.0143	5.683 (4.831)	10.705 (10.344)	8.054 (7.952)	-45.5 (-60.4)	2.28
	HB3	2.311 (2.312)	0.0261	0.0135					
[H6L]I ₂	HB1	2.571 (2.548)	0.0209	0.0128					2.20
	HB2	2.509 (2.493)	0.0245	0.0134	5.435 (4.821)	10.502 (10.252)	8.347 (8.102)	-45.7 (-63.8)	
	HB3	2.571 (2.548)	0.0209	0.0128					

Notes: $\rho(\text{BCPs})$: density of the bond critical points. $\nabla^2\rho$: Laplacian of the density at the bond critical points. H: the distance between the two benzene planes. ΔE : binding energies of the complex $[\text{H}_6\text{L}(\text{X})_2]^{4+}$, $\Delta E = E([\text{H}_6\text{L}(\text{X})_2]^{4+}) - E([\text{H}_6\text{L}]^{6+}) - 2E(\text{X})^-$. $\log K_2$: binding data of the ligand for halides in D₂O at 298K. (Reference [19]).

The atomic distance of N1H...Cl1 and N3H...Cl1 for HB1 and HB3 is both calculated to be 2.147 Å. Their density of the BCP is 0.0296 au while the Laplacian of the density is about 0.0171 au. HB2 reveals a shorter atomic distance of 2.068 Å. The density of the BCP and the Laplacian of the density are larger than those of HB1 and HB3, which read as 0.0368 au and 0.0181 au, respectively.

These values are typical for the descriptions of hydrogen bonding [34,35]. HB2 is characterized by a stronger hydrogen bond than HB1 and HB3, which is also confirmed by X-ray data where the Cl ion is closer to N2 than to N1 and N3.

The deformation electron density maps for the three H bonds (Figure 2b–d) clearly demonstrate the typical characteristics of the H bonds. The electron density increases between the donating protons and the chloride anion. The electron density increase along HB2 is larger than that of the HB1 and HB3, indicating that hydrogen bond HB2 is strong than the other two. This observation is consistent to the shorter H . . . Cl atomic distance in HB2 than that in HB1 and HB3. The electron density difference map of $[H_6LCl_2]^{4+}$ also shows a decrease in density at the proton position H and at the lone electron pair of N for all three hydrogen bonds. The binding energy in $[H_6LCl_2]^{4+}$ suggests that the average H bonding amounts to 8~9 kcal/mol.

3.2. Two Bromides Encapsulated in $[H_6L]^6$

It should be noted here that the crystallography results are available only for $[H_4L(Br)_2]^{2+}$ and $[H_4LI_2]^{2+}$ where N2 and N5 are not protonated. The experimental data reveal that bromides and iodides are not encapsulated in the azamacrocyclic cavity (see supplementary materials). For comparison and consistency purposes, in the present study, we consider the six protonated azamacrocyclic cavity for all the models as those in reference [19].

As depicted in Figure 3a, the optimized structure of compound $[H_6LBr_2]^{4+}$ has a C_{2h} symmetric geometry. The size of the azamacrocyclic cavity in this compound is measured by width of 10.705 Å and height of 8.054 Å, which show that the paralleled aromatic benzene planes are parted farther, and N2 and N5 becomes closer with a shorter atomic distance when comparing to those of $[H_6LCl_2]^{4+}$ complexes. The two bromides are separated by about 5.683 Å. The atomic distance of N1H . . . Br and N3H . . . Br for HB1 and HB3 are calculated to be 2.311 Å and 2.309 Å, respectively. Both of the corresponding densities of BCPs is ~0.026 au and the Laplacian of density through AIM analysis is around 0.013 au. Comparison with HB1 and HB3, HB2 demonstrates a shorter atomic distance for N2H . . . Br (2.233 Å) and a larger density of BCP (0.0319 au) and a larger Laplacian of density (0.0143). This implies that hydrogen bond HB2 is stronger than hydrogen bonds of HB1 and HB3. The electron density differences maps also reveal a stronger HB2, where the electron density increases along N2H . . . Br of HB2 (Figure 4c) more than those along N1H . . . Br of HB1 and N3H . . . Br of HB3 (Figure 3b,d).

The binding energies for the two bromides in $[H_6LBr_2]^{4+}$ is calculated to be -45.5 kcal/mol in the solvent, which is about 7 kcal/mol weaker than the binding of $[H_6LCl_2]^{4+}$.

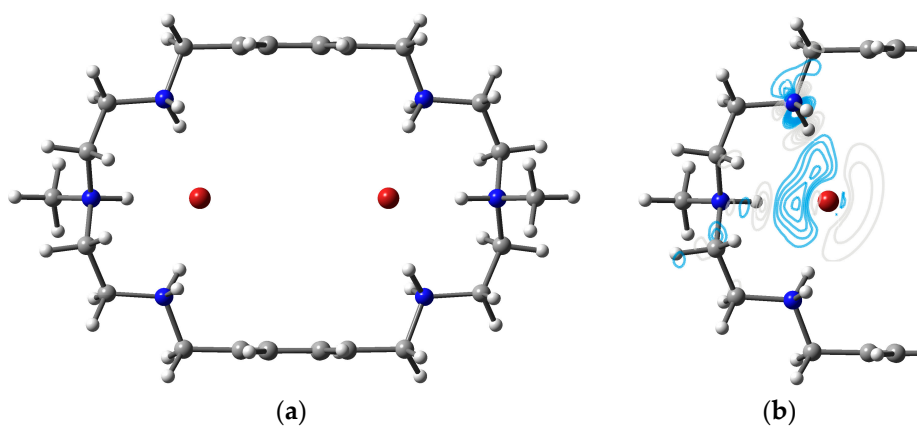


Figure 3. Cont.

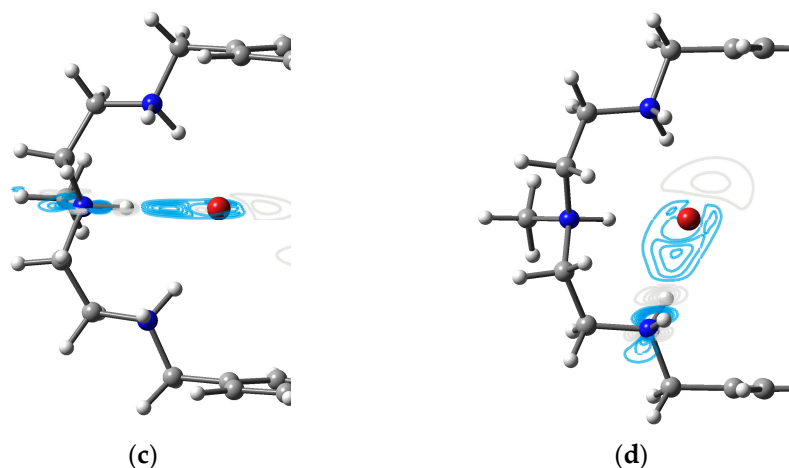


Figure 3. Two bromides encapsulated by the azamacrocyclic compound. (a) Optimized $[\text{H}_6\text{LBr}_2]^{4+}$ structure; (b) electron density differences ($\Delta\rho$) maps of HB1 in the plane of N1–H–Br1; (c) electron density differences ($\Delta\rho$) maps of HB2 in the plane of N2–H–Br1; and (d) electron density differences ($\Delta\rho$) maps of HB3 in the plane of N3–H–Br1. Contours in the deformation density map are shown at ± 0.001 au. Grey lines indicate deficiency of density, and blue lines indicate increasing density. $(\Delta\rho) = \rho[\text{H}_6\text{LBr}_2]^{4+} - \rho[\text{H}_6\text{L}]^{6+} - \rho(\text{Br}_2)^{2-}$.

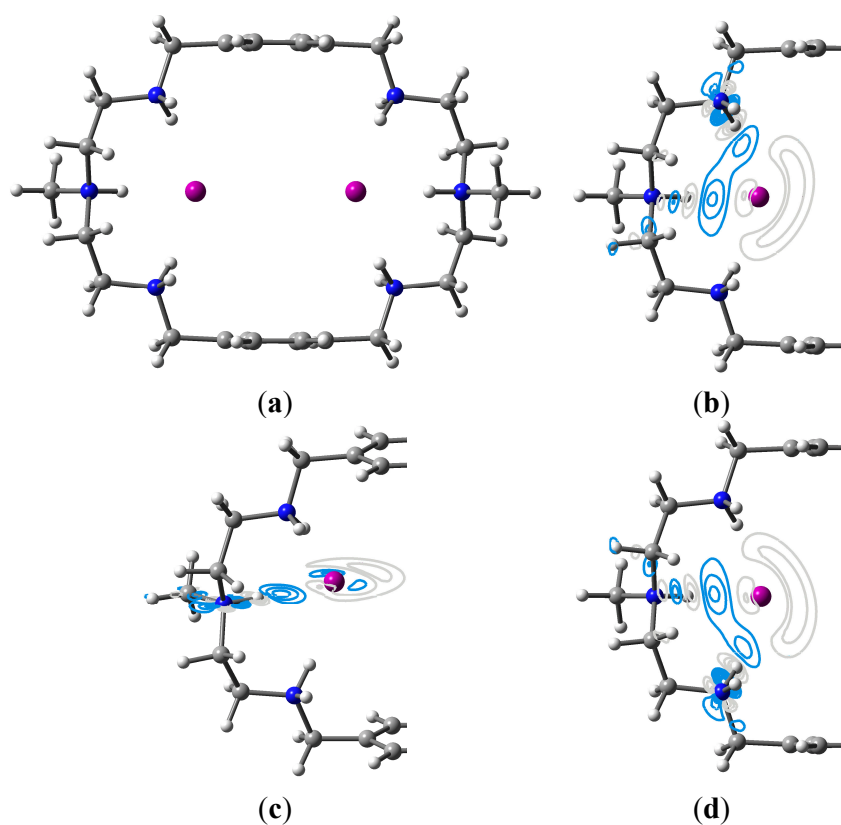


Figure 4. Two iodides encapsulated by the azamacrocyclic compound. (a) Optimized $[\text{H}_6\text{LI}_2]^{4+}$ structure; (b) electron density differences ($\Delta\rho$) maps of HB1 in the plane of N1–H–I1; (c) electron density differences ($\Delta\rho$) maps of HB2 in the plane of N2–H–I1; and (d) electron density differences ($\Delta\rho$) maps of HB3 in the plane of N3–H–I1. Contours in the deformation density map are shown at ± 0.001 au. Grey lines indicate deficiency of density, and blue lines indicate increasing density. $(\Delta\rho) = \rho[\text{H}_6\text{LI}_2]^{4+} - \rho[\text{H}_6\text{L}]^{6+} - \rho(\text{I}_2)^{2-}$.

3.3. Two Iodides Encapsulated in $[H_6L]^6$

The azamacrocycle cavity which encapsulates two iodide anions has a size characterized by a width of 10.502 Å and a height of 8.347 Å. The atomic distance between the two iodides is 5.435 Å. The bond distances for NH...I are predicted to be 2.573 Å, 2.509 Å, and 2.571 Å for HB1, HB2, and HB3, respectively. This shows that HB2 is stronger than HB1 and HB3. The same feature can also be seen in the related electron density difference maps (Figure 4b–d). The density of BCP for HB2 is 0.0245 au, which is about 0.004 au larger than those of HB1 and HB3, while the Laplacian of density for HB2 is 0.0134 au, which is slightly larger than those of HB1 and HB3.

The binding energy of -45.7 kcal/mol characterizes complexes between iodides and the azamacrocycle. This shows similar binding strength as that predicted for analogous complex with bromide anions, while it has weaker binding characteristics than those of chloride anions.

3.4. Two Fluorides Encapsulated in $[H_6L]^6$

The PCM model optimized structure of model $[H_6LF_2]^{4+}$ complex is shown in Figure 5a. For this compound, the width of the azamacrocycle cavity is calculated to be 11.314 Å. The height is predicted to be 7.119 Å. The overall shape is elongated for the $[H_6LF_2]^{4+}$ complex, as compared to the other complexes. This elongation is partly due to the stronger charge repulsion between the F anions. This can be further confirmed by the significant separation of the two F anions in the complex. The two fluoride anions are encapsulated inside the cavity at the two corners. The atomic distance between the two anions is estimated to be 6.563 Å. For the comparison, the other halide anions in the cavity are separated by less than 5.7 Å. As depicted in Figure 5, each fluoride anion is bounded within the cavity through three hydrogens of the nearby protonated amine nitrogens. Compared to the other halide complexes, the HBs in $[H_6LF_2]^{4+}$ complex are significantly shorter than those found in other halides complexes. For hydrogen bonds 1 and 3 (HB1 and HB3), the atomic distances of N1H...F1 is 1.612 Å.

Based upon the AIM analysis, the density of the bond critical point (BCP) for HB1 (or HB3) is about 0.0514 au and the corresponding Laplacian of the density is predicted to be 0.0414 au. This suggests that HB1 is a strong hydrogen bond. The atomic distance of N2H...F1 of HB2 is measured to be 1.510 Å, which is about 0.1 Å shorter than that of HB1. The density of BCP and the Laplacian of the density of HB2 are calculated to be 0.0691 au and 0.0485 au, respectively (Table 1). Here one can see that the density of BCP of HB2 is about 0.018 au larger than that of HB1 or HB3. This large BCP density suggests that the corresponding bond should not be attributed to the H bond only.

To explore the nature of this extraordinary N–H–F interaction the analysis of the electron density differences of this complex has been performed. The deformation density maps for the three hydrogen bonds (HB1, HB2, and HB3) are depicted in Figure 5. The electronic structures of the H-bond reveal themselves in the deformation density map of $[H_6LF_2]^{4+}$. For HB1 and HB3 (Figure 5b,d), it can be seen that the concentration of electron density arises between the proton H and the proton acceptor (fluoride) with a corresponding electron density deficiency at the positions of the proton H and the acceptor lone pair of nitrogen. For HB2, the electron density deformation map (Figure 5c) shows an inescapable difference as compared to those of HB1 and HB3. The electron density increase on the N–H–F plane is not just limited to the space between H and F atomic centers. The electron density increase is surrounding the fluoride center in this HB2 bond plane. Moreover, the electron density increase along H-bond HB2 is much larger compared to that of the H bonds of HB1 and HB3. This implies that HB2 is a much stronger hydrogen bond than HB1 and HB3. These differences are well correlated with the notable short atomic distance of 1.510 Å for HB2. The density of BCP (around 0.07) also shows a bigger density than the regular hydrogen bonds. Considering these factors, one can describe HB2 as a hybrid hydrogen bond combined with some character of ionic bonding between the proton and the fluoride. Therefore, HB2 contributes to the binding more than HB1 and HB3.

The binding energies for the two fluorides anions with $[H_6L]^{6+}$ are calculated to be about -95.9 kcal/mol in polarizable environments, suggesting a very strong binding for the fluorides and the azamacrocycle cavity. This provides further proof that HB2 is not just a pure hydrogen bond, but

a hybrid hydrogen bond augmented with ionic binding which shows a much stronger binding than those of HB1 and HB3.

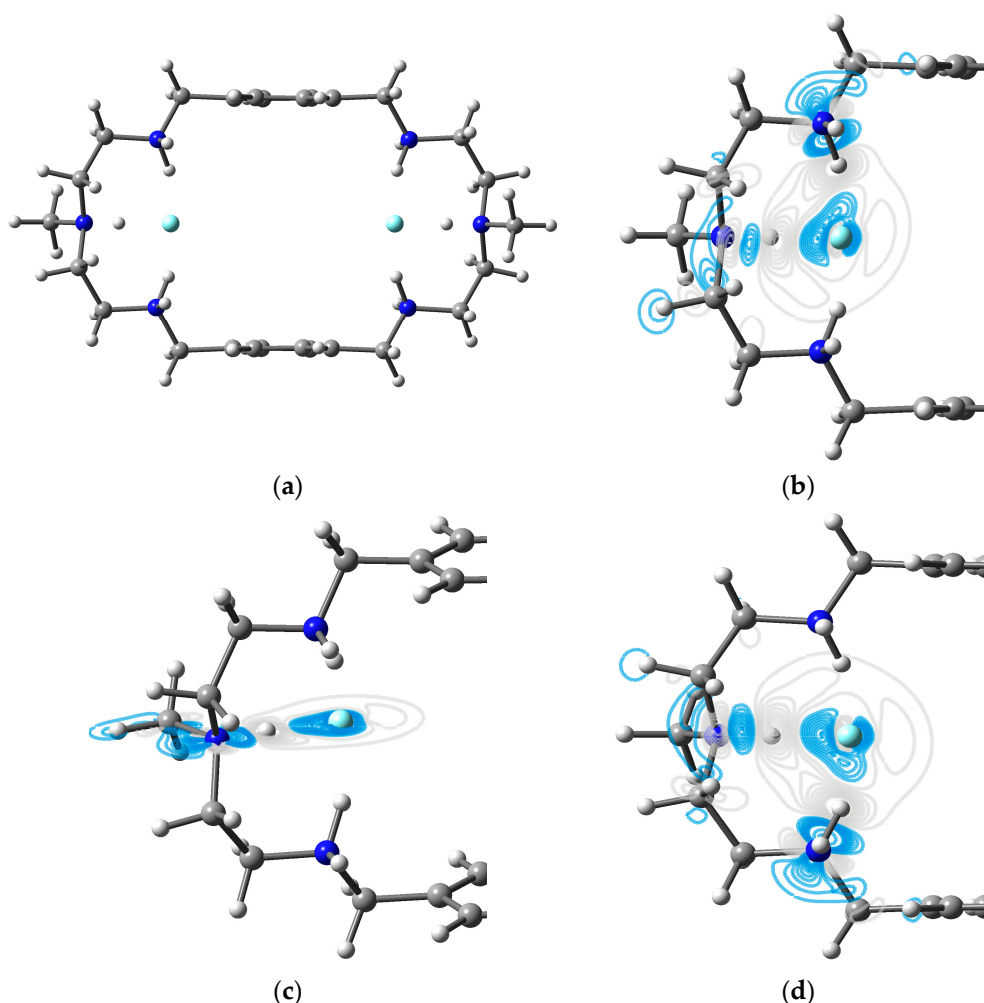


Figure 5. Two fluorides encapsulated by the azamacrocyclic compound. (a) Optimized $[\text{H}_6\text{LF}_2]^{4+}$ structure; (b) electron density differences ($\Delta\rho$) maps of HB1 in the plane of N1–H–F1; (c) electron density differences ($\Delta\rho$) maps of HB2 in the plane of N2–H–F1; and (d) electron density differences ($\Delta\rho$) maps of HB3 in the plane of N3–H–F1. Contours in the deformation density map are shown at ± 0.001 au. Grey lines indicate deficiency of density, and blue lines indicate increasing density. $\Delta\rho = \rho([\text{H}_6\text{LF}_2]^{4+}) - \rho([\text{H}_6\text{L}]^{6+}) - \rho(\text{F}_2)^{2-}$.

As shown in the binding ligand–halides data for the 1:2 binding complexes at 298K in D2O (Table 1), the calculated binding strength of the studied species has the same trend as observed in experiments. The fluorides have the strongest binding of all the considered species and the chlorides have the less pronounced binding potential.

There is significant influence of the complexation of halide ions on the structure of azamacrocyclic. It is noted that the cavity of azamacrocyclic ring becomes larger in order to accommodate the halides. The fluorides complex is characterized by the longest width and the shortest height of the cavity, while in the iodides complex has the narrowest width and the longest height. Due to the strong charge repulsion, the two fluoride ions are located at the largest distance apart, about 1 Å farther than the other three halides species. The binding energy suggests that the fluorides have the strongest binding affinity to the receptor's cavity.

4. Conclusions

The structural and bonding characteristics of halide ion complexes with an azamacrocycle have been investigated using a computational, DFT-based approach. We observed that the cavity of an azamacrocycle ring expands in order to accommodate the halides. The fluoride complex has the longest width and the shortest height of the cavity while the iodide complex is characterized by the narrowest width and the longest height. Due to the strong charge repulsion, the two fluorides are located at the largest distance apart, about 1 Å farther than the other three halides species. The values of binding energy suggest that the fluorides have the strongest interactions with the azamacrocycle. As investigated by the electron density analysis, the interaction between NH–F is not limited to traditional H bonding, but it could be described as a hybrid hydrogen bond mixed with contributions of ionic bonding between the proton and the fluoride. On the other hand, the binding strength of the chloride, bromide, and iodide complexes is only half (or less) of that of the fluorides. The electron density analysis indicates that the halides in these complexes are stabilized through the normal hydrogen bonds.

Supplementary Materials: The supplementary materials are available online at <http://www.mdpi.com/2073-4352/6/3/31/s1>.

Acknowledgments: The authors thank for support of the NSF CREST Interdisciplinary Nanotoxicity Center NSF-CREST—Grant # HRD-0833178; NSF-EPSCoR Award Number: 362492-190200-01-0903787. The computation time was provided by the Extreme Science and Engineering Discovery Environment (XSEDE) by National Science Foundation Grant Number OCI-1053575 and XSEDE award allocation Number DMR110088 and by the Mississippi Center for Supercomputer Research.

Author Contributions: Jing Wang and Jerzy Leszczynski conceived and designed the theoretical study; Md. Alamgir Hossain performed the experiments; Jing Wang performed the calculations; Jing Wang and Jiande Gu analyzed the data; Jing Wang wrote the paper.

Conflicts of Interest: The authors declare no conflict of interest.

References

1. Wenzel, M.; Hiscock, J.R.; Gale, P.A. Anion receptor chemistry: Highlights from 2010. *Chem. Soc. Rev.* **2012**, *41*, 480–520. [[CrossRef](#)] [[PubMed](#)]
2. Bianchi, A.; Bowman-James, K.; Garcia-Espana, E. *Supramolecular Chemistry of Anions*; Wiley: New York, NY, USA, 1997.
3. Amendola, V.; Esteban-Gomez, D.; Fabbrizzi, L.; Licchelli, M. What anions do to N–H-Containing Receptors. *Acc. Chem. Res.* **2006**, *39*, 343–353. [[CrossRef](#)] [[PubMed](#)]
4. Wichmann, K.; Antonioli, B.; Sohnel, T.; Wenzel, M.; Gloe, K.; Gloe, K.; Price, J.R.; Lindoy, L.F.; Blake, A.J.; Schroder, M. Pylymine-based anion receptors: Extraction and structural studies. *Coord. Chem. Rev.* **2006**, *250*, 2987–3003. [[CrossRef](#)]
5. Hossain, M.A. Inclusion complexes of halide anions with macrocyclic receptors. *Curr. Org. Chem.* **2008**, *12*, 1231–1256. [[CrossRef](#)]
6. Révész, Á.; Schröder, D.; Svec, J.; Wimmerová, M.; Sindelar, V. Anion binding by bambus[6]uril probed in the gas phase and in solution. *J. Phys. Chem. A* **2011**, *115*, 11378–11386. [[CrossRef](#)] [[PubMed](#)]
7. Pramanik, A.; Powell, D.R.; Wong, B.M.; Hossain, M.A. Spectroscopic, structural, and theoretical studies of halide complexes with a urea-based tripodal receptor. *Inorg. Chem.* **2012**, *51*, 4274–4284. [[CrossRef](#)] [[PubMed](#)]
8. Turner, D.R.; Paterson, M.J.; Steed, J.W. A conformationally flexible, urea-based tripodal anion receptor: solid-state, solution, and theoretical studies. *J. Org. Chem.* **2006**, *71*, 1598–1608. [[CrossRef](#)] [[PubMed](#)]
9. Chen, Y. Theoretical study of interactions between halogen-substituted s-triazine and halide anions. *J. Phys. Chem. A* **2013**, *117*, 8081–8090. [[CrossRef](#)] [[PubMed](#)]
10. Chaumont, A.; Wipff, G. Macrotricyclic quaternary tetraammonium receptors: Halide anion recognition and interfacial activity at an aqueous interface. A molecular dynamics investigation. *J. Comput. Chem.* **2002**, *23*, 1532–1543. [[CrossRef](#)] [[PubMed](#)]

11. Wang, D.X.; Zheng, Q.Y.; Wang, Q.Q.; Wang, M.X. Halide recognition by tetroxalix[2]arene[2]triazine receptors: Concurrent nocovalent halide- π and lone-pair- π interactions in host-halide-water ternary complexes. *Angew. Chem. Int. Ed. Engl.* **2008**, *47*, 7485–7488. [[CrossRef](#)] [[PubMed](#)]
12. Liu, Y.-Z.; Yuan, K.; Lv, L.-L.; Zhu, Y.-C.; Yuan, Z. Designation and exploration of halide-anion recognition based on cooperative nocovalent interactions including hydrogen bonds and anion- π . *J. Phys. Chem. A* **2015**, *119*, 5842–5852. [[CrossRef](#)] [[PubMed](#)]
13. Rhaman, M.M.; Ahmed, L.; Wang, J.; Powell, D.R.; Leszczynski, J.; Hossain, M.A. Encapsulation and selectivity of sulfate with a furan-based hexaazamacrocyclic receptor in water. *Organ. Biomol. Chem.* **2014**, *12*, 2045–2048. [[CrossRef](#)] [[PubMed](#)]
14. Valencia, L.; Bastida, R.; García-España, E.; de Julián-Ortiz, J.V.; Llinares, J.M.; Macías, A.; Pérez Lourido, P. Nitrate encapsulation within the cavity of polyazapyridinophane. Considerations on nitrate-pyridine interactions. *Cryst. Growth Des.* **2010**, *10*, 3418–3423. [[CrossRef](#)]
15. Chauhan, S.M.S.; Garg, B.; Bisht, T. Synthesis and anion binding of 2-Arylalazo-meso-octamethylcalix[4]pyrroles. *Supramol. Chem.* **2009**, *21*, 394–400. [[CrossRef](#)]
16. Juwarker, H.; Lenhardt, J.M.; Castillo, J.C.; Zhao, E.; Krishnamurthy, S.; Jamiolkowski, R.M.; Kim, K.-H.; Graig, S.L. Anion binding of short, flexible aryl triazole oligomers. *J. Org. Chem.* **2009**, *74*, 8924–8934. [[CrossRef](#)] [[PubMed](#)]
17. Mendy, J.S.; Pilate, M.L.; Horne, T.; Dey, V.W.; Hossain, M.A. Encapsulation and selective recognition of sulfate anion in an azamacrocycle in water. *Chem. Commun.* **2010**, *46*, 6084–6086. [[CrossRef](#)] [[PubMed](#)]
18. Hossain, M.A.; Saeed, M.A.; Fronczek, F.R.; Wong, B.M.; Deay, K.R.; Mendy, J.S.; Gibson, D. Charge-assisted encapsulation of two chlorides by a hexaprotonated azamacrocycle. *Cryst. Growth Des.* **2010**, *10*, 1478–1481. [[CrossRef](#)] [[PubMed](#)]
19. Ahmed, L.; Rhaman, M.M.; Mendy, J.S.; Wang, J.; Fronczek, F.R.; Powell, D.R.; Leszczynski, J.; Hossain, M. Experimental and theoretical studies on halide binding with a p-Xylyl-based azamacrocycle. *J. Phys. Chem. A* **2015**, *119*, 383–394. [[CrossRef](#)] [[PubMed](#)]
20. Becke, A.D. Density-functional thermochemistry. III. The role of exact exchange. *J. Chem. Phys.* **1993**, *98*, 5648–5652. [[CrossRef](#)]
21. Bader, R.F.W. *Atoms in Molecules: A Quantum Theory*; Clarendon Press: Oxford, UK, 1990.
22. Bader, R.F.W. A quantum theory of molecular structure and its applications. *Chem. Rev.* **1991**, *91*, 893–928. [[CrossRef](#)]
23. Lee, C.; Yang, W.; Parr, R.G. Development of the Colle-Salvetti correlation-energy formula into a functional of the electron density. *Phys. Rev. B* **1988**, *37*, 785–789. [[CrossRef](#)]
24. Stephens, P.J.; Devlin, F.J.; Chabalowski, C.F.; Frisch, M.J. Ab initio calculation of vibrational absorption and circular dichroism spectra using density functional force fields. *J. Phys. Chem.* **1994**, *98*, 11623–11627. [[CrossRef](#)]
25. Miehlich, B.; Savin, A.; Stoll, H.; Preuss, H. Results obtained with the correlation energy density functionals of becke and Lee, Yang and Parr. *Chem. Phys. Lett.* **1989**, *157*, 200–206. [[CrossRef](#)]
26. Zhao, Y.; Truhlar, D.G. Applications and validations of the minnesota density functional. *Chem. Phys. Lett.* **2011**, *502*, 1–13. [[CrossRef](#)]
27. Zhao, Y.; Truhlar, D.G. The M06 suite of density functional for main group thermochemistry, thermochemical kinetics, nocovalent interactions, excited states, and transition elements: two new functional and systematic testing of four M06-class functional and 12 other functional. *Theor. Chem. Acc.* **2008**, *120*, 215–241. [[CrossRef](#)]
28. Zhao, Y.; Truhlar, D.G. Density functional with broad applicability in chemistry. *Acc. Chem. Res.* **2008**, *41*, 157–167. [[CrossRef](#)] [[PubMed](#)]
29. Hehre, W.J.; Radom, L.; Schleyer, P.R.; Pople, J.A. *Ab initio Molecular Orbital Theory*; Wiley: New York, NY, USA, 1986.
30. Cossi, M.; Barone, V.; Cammi, R.; Tomasi, J. Ab initio study of solvated molecules: A new implementation of the polarizable continuum model. *Chem. Phys. Lett.* **1996**, *255*, 327–335. [[CrossRef](#)]
31. Frisch, M.J.; Trucks, G.W.; Schlegel, H.B.; Scuseria, G.E.; Robb, M.A.; Cheeseman, J.R.; Scalmani, G.; Barone, V.; Mennucci, B.; Petersson, G.A.; et al. *Gaussian 09, Revision D.01*; Gaussian, Inc.: Wallingford, CT, USA, 2009.
32. Biegler-König, F.; Schönbohm, J.; Bayles, D. AIM2000—A program to analyze and visualize atoms in molecules. *J. Comput. Chem.* **2001**, *22*, 545–559.

33. Vanquickenborne, L.G. Quantum chemistry of hydrogen bonds. In *Intermolecular Forces*; Huyskens, P.L., Luck, W.A.P., ZeegersHuyskens, T., Eds.; Springer: Berlin/Heidelberg, Germany, 1991; p. 41.
34. Grabowski, S.J.; Leszczynski, J. Unrevealing the nature of hydrogen bonds: PI-electron delocalization shapes H-Bond features. Intramolecular and intermolecular resonance-assisted hydrogen bonds in hydrogen bonding new insights. In *Challenges and Advances in Computational Chemistry and Physics*; Leszczynski, J., Ed.; Springer: Dordrecht, The Netherlands, 2006; Volume 3.
35. Lipkowski, P.; Grabowski, S.J.; Leszczynski, J. Properties of the halogen-hydride interaction: An ab initio and “atoms in molecules” analysis. *J. Phys. Chem. A* **2006**, *110*, 10296–10302. [[CrossRef](#)] [[PubMed](#)]



© 2016 by the authors; licensee MDPI, Basel, Switzerland. This article is an open access article distributed under the terms and conditions of the Creative Commons by Attribution (CC-BY) license (<http://creativecommons.org/licenses/by/4.0/>).